



## Sustained-release capsules coated via thermoforming techniques

Lian Shen<sup>a</sup>, Xiaohong Yu<sup>b</sup>, Hui Fu<sup>a</sup>, Sainan Wei<sup>a</sup>, Weiguang Shan<sup>a</sup>, Yan Yang<sup>a,\*</sup>

<sup>a</sup> College of Pharmaceutical Science, Zhejiang University of Technology, Hangzhou, China

<sup>b</sup> Air Force Healthcare Center for Special Services Hangzhou, Hangzhou, China

### ARTICLE INFO

#### Keywords:

Capsule coating  
Vacuum forming coating  
Centrifugal forming coating  
Sustained-release  
Thickness distribution

### ABSTRACT

Capsule coatings have a wide range of applications as they afford protection to active pharmaceutical ingredients. However, few studies have focused on capsule coating owing to the sensitivity of hard gelatin shells to solvents and high temperature. In the present study, we aimed to coat capsules using two thermoforming coating techniques: vacuum forming coating (VFC) and centrifugal forming coating (CFC). Rheological and mechanical properties were investigated to comprehensively elucidate the processes and mechanisms underlying the two coating techniques. The corresponding coating integrity and drug release behavior were characterized and compared. Herein, we observed that a lower temperature was more suitable for the VFC process than the CFC process. The drug release rate decreased with the film thickness increased. Both optimal VFC and CFC capsules revealed a 24 h sustained-release property following Fick's diffusion law. The coating thickness distribution was more homogeneous for the VFC capsule than the CFC capsule. With the advantage solvent-free of functional capsule coatings, thermoforming coating techniques are convenient and efficient solutions for small-scale personalized coating of oral solid preparations.

### 1. Introduction

Capsule coatings have a wide range of applications in the manufacture of sustained-release, delayed-release, and pulsatile-release capsules. However, hard gelatin shells are unstable in aqueous and organic solvents. Even when coating conditions are stringently controlled, sticking and rupture of the hard gelatin shells occur easily. To date, successful capsule coatings using liquid-based coating techniques have rarely been reported. For example, an aqueous ethylcellulose dispersion (Aquacoat® ECD) was used to prepare pulsatile capsules (Mohamad and Dashevsky, 2006); Eudragit® L 30 D-55 dispersion was used to prepare enteric capsules (Macchi et al., 2016), and Eudragit® S 100 dissolved in isopropyl alcohol: acetone (20:14.5, v/v) mixture was used to prepare enteric capsules (Deshmukh et al., 2020). Solvent-free coating techniques, such as compression coating (Tang et al., 2018), hot-melt coating (Yang et al., 2017), dry powder coating (Terebesi and Bodmeier, 2010; Yang et al., 2015), and photocurable coating (Bose and Bogner, 2010), provide feasible strategies to resolve instability issues associated with hard gelatin shells in contact with solvents. Considering that capsule cores fail to withstand the high pressure during compression coating or high temperature during hot-melt coating, more limitations should be examined during the capsule coating than during the

tablet coating.

In our previous study, electrostatic dry powder coating (EDPC) was used to prepare sustained-release capsules, revealing higher production efficiency and better stability than the solvent-based coating method (Yang et al., 2018). However, the EDPC method is highly dependent on the particle size of the ultrafine coating powder (10–80 μm), as well as the electrical resistance of the capsule cores ( $< 1 \times 10^9$  mΩ) (Bose and Bogner, 2007). The coating process involved spraying the plasticizer and then the coating powder; these steps were repeated several times until the required coating level was obtained. If various films could be prefabricated by the solution casting method and used to coat over the capsule core layer-by-layer, or if the film with different materials and thicknesses could be prefabricated to coat over the capsule core directly, the efficiency and quality of the coating would be greatly improved.

Thermoforming is a commonly used plastic processing technique with the advantages of simplicity, low cost, and high performance (Hosseini et al., 2007). During the thermoforming process, a thermo-plastic sheet is softened by heating and deformed along with the mold under vacuum pressure (Leite et al., 2018; Seefried et al., 2016) or mechanical force (Hosseini et al., 2010). Recently, osmotic pump tablets were prepared by separately calendaring cellulose acetate coating membranes on tablet cores under mechanical force (Yuan et al., 2019). The results suggested that using the thermoforming technique to

\* Corresponding author.

E-mail address: [yangyan10@zjut.edu.cn](mailto:yangyan10@zjut.edu.cn) (Y. Yang).

<https://doi.org/10.1016/j.ejps.2021.106050>

Received 21 April 2021; Received in revised form 25 September 2021; Accepted 25 October 2021

Available online 28 October 2021

0928-0987/© 2021 The Authors.

Published by Elsevier B.V. This is an open access article under the CC BY-NC-ND license

(<http://creativecommons.org/licenses/by-nc-nd/4.0/>).

Nomenclature		
EDPC	electrostatic dry powder coating	electron microscopy
VFC	vacuum forming coating	$P_{vmin}$ minimum operating vacuum pressure
CFC	centrifugal forming coating	$Q$ cumulative drug release
RS	Eudragit® RS PO	$\Delta P_v$ operating vacuum pressure range
RL	Eudragit® RL PO	$T_g$ glass transition temperature
MT	metoprolol tartrate	$T_{cmi}$ minimum operating temperature for CFC
MCC	microcrystalline cellulose	$dQ/dt$ drug release rate
TEC	triethyl citrate	$T_{cmax}$ maximum operating temperature for CFC
$P_v$	vacuum pressure	$A_s$ surface area
$T_{vmin}$	minimum operating temperature for VFC	$\Delta T_c$ operating temperature range for CFC
$T_{vmax}$	maximum operating temperature for VFC	$D$ diffusion coefficient
$\Delta T_v$	operating temperature range for VFC	$S_{min}$ minimum rotational speed
		$K$ drug distribution coefficient between film and core
		$P_c$ centrifugal pressure
		$d$ coating thickness
		$m$ weight of the film
		$\Delta C$ drug concentration difference inside and outside the coating
		$S$ rotational speed
		DSC differential scanning calorimetry
		$r$ radius of the centrifugal ring

produce a solid preparation coating could prevent organic solvent volatilization, avoid dust pollution, and shorten the operation time. However, a thermoforming coating based on mechanical force necessitates mechanical strength of the inner core and is only suitable for tablet coating. Thus, thermoforming coatings under vacuum pressure and centrifugal pressure might be an alternative strategy to produce capsule coatings that maintain the integrity and stability of the capsule core.

For the thermoforming products, the coating thickness distribution is an important index for quality evaluation (Cha et al., 2019). First, process parameters, such as heating temperature and heating time, are known to affect the thickness distribution. The lowest temperature area reportedly shows a more uniform thickness distribution than the highest temperature area in the vacuum snap-back-forming process (Lee et al., 2001b). With a prolonged heating time, the temperature-sensitive acrylonitrile butadiene styrene polymers demonstrate a greater thickness deviation (Nam and Lee, 2016). Second, material properties, including rheological properties and friction between the mold and film, also affect the thickness distribution. For example, polymers with higher elongational viscosity and greater strain hardening exhibit a more uniform thickness distribution (Lee et al., 2001a). The higher the friction between the plug and sheet, the more uniform the thickness distribution achieved during the plug-assisted thermoforming process (Morales et al., 2014). Finally, mold properties, such as mold type and fixture shape, are also important. For the female mold, increasing the heating time benefits the uniform thickness distribution of the high-impact polystyrene cups. In contrast, decreasing the heating time was crucial for a uniform thickness distribution with the male mold (Ghobadnam et al., 2014). Furthermore, a circular clamping tool can generate a more uniform thickness distribution of cylindrical and conical products than a rectangular one (Erdogan and Eksi, 2014). In addition to the thickness distribution, the coating integrity and function are important quality evaluation indicators. Therefore, to promote the application of thermoforming technology in the biomedical field, it is necessary to investigate the coating formation process and various influencing factors.

In the present study, two thermoforming coating techniques, vacuum forming coating (VFC) and centrifugal forming coating (CFC), were evaluated for the possibility in capsule coating. Eudragit® RS PO (RS)/RL PO (RL) with different plasticizer concentrations were used as a sustained-release coating film. The coating temperature and pressure were optimized to achieve integral-coated capsules. The rheological and mechanical properties of the coating films were assessed to gain a better understanding of the thermoforming process. Furthermore, the coating thickness distribution under vacuum pressure and centrifugal pressure was evaluated.

## 2. Material and methods

### 2.1. Material

Metoprolol tartrate (MT; No. 1015-1802001) was supplied by Apeloa JiaYuan Pharmaceutical Co., Ltd. (Zhejiang, China). Lactose (Granulac® 70, No. L1145) was obtained from Meggle Group (Wasserburg, Germany). Microcrystalline cellulose (MCC; No. 20131103) was purchased from Yingkou AODA Pharmaceutical Co., Ltd. (Liaoning, China). RS (No. G140338038) & RL (No. G131136140) were purchased from Evonik Industries AG (Essen, Germany). Triethyl citrate (TEC; No. 181126) was kindly donated by Fengyuan Tushan Pharmaceutical Co., Ltd. (Anhui, China). Hard gelatin shell (No. 1, No. 20180323) was kindly donated by Shaoxing Kangke Capsule Co., Ltd. (Zhejiang, China). Reagent-grade ethanol was purchased from Huipu Chemical & Apparatus Co., Ltd. (Hangzhou, China).

### 2.2. Preparation of polymer films and uncoated capsules

RS and RL were mixed, and TEC was added as a plasticizer based on the polymer weight. The mixture was dissolved in ethanol, and the formulations are listed in Table 1. Approximately 7 mL of the above solution was poured onto a Teflon plate (70 mm × 90 mm) and then airdried at room temperature (Hoffmann et al., 2011). The obtained films were cut into rectangular specimens for further use. MT (20%, w/w), lactose (50%, w/w), and MCC (30%, w/w) were manually mixed, passed thrice through an 80-mesh sieve, and filled into hard gelatin shells to prepare uncoated capsules (approximately 50 mg MT per capsule).

**Table 1**

Formulations of solutions to prepare polymer films.

No.	RS (g)	RL (g)	TEC (g)	Ethanol (mL)
Rx1	4.8	1.2	0.9	40
Rx2			1.2	
Rx3			1.5	
Rx4			1.8	
Rx5	5.4	0.6	1.2	40
Rx2	4.8	1.2		
Rx6	3.0	3.0		
Rx7	3.2	0.8	0.8	40
Rx2	4.8	1.2	1.2	
Rx8	8.0	2.0	2.0	

### 2.3. Preparation of coated capsules by VFC

The polymer films were cut into rectangular specimens (35 mm × 55 mm). Two polymer film pieces were placed in the middle of the self-made mold, with the capsule core placed inside (Fig. 1a); two vent holes were present on both sides of the middle part. Talc was added as a lubricant between the mold and films to prevent adhesion. A schematic of the VFC process is shown in Fig. 1b. The mold was fixed with screws and heated at different temperatures (increased at 1 °C per run) for 5 min, and then different vacuum pressures ( $P_v$ ) (increased at 2 kPa per run) were applied for 1 min. The capsule was removed after the  $P_v$  was withdrawn, and the excess film was cut to obtain the VFC capsule. The minimum operating temperature for VFC, at which the capsule was completely coated, was recorded as  $T_{vmin}$ , while the maximum operating temperature for VFC, at which the capsule sagged to the bottom, was recorded as  $T_{vmax}$ . The difference between  $T_{vmax}$  and  $T_{vmin}$  was recorded as the operating temperature range ( $\Delta T_v$ ). The minimum operating vacuum pressure for VFC, at which the capsule was completely coated, was recorded as  $P_{vmin}$ , while the difference in  $P_{vmin}$  and 100 kPa (maximum value of  $P_v$ ) was recorded as the operating vacuum pressure range ( $\Delta P_v$ ).

### 2.4. Preparation of coated capsules by CFC

The polymer films were cut into rectangular specimens (35 mm × 45 mm). Two polymer film pieces were pasted inside the centrifugal ring, with the capsule core placed between the film pieces (Fig. 1c). The operating temperature was monitored using an infrared temperature sensor, and a lid was added to maintain a stable temperature. A schematic of the CFC process is shown in Fig. 1d. The heating chamber was heated at different temperatures (increased at 5 °C per run) for 5 min, and then rotated at different speeds (increased at 25 rpm per run) for 1 min. The capsule was removed after the rotational speed was withdrawn, and the excess film was cut to obtain the CFC capsule. The minimum operating temperature for CFC, at which the capsule was completely coated, was recorded as  $T_{cmin}$ , while the maximum operating temperature for CFC, at which the hard gelatin shell became soft and

deformed, was recorded as  $T_{cmax}$ . The difference between  $T_{cmax}$  and  $T_{cmin}$  was recorded as the operating temperature range ( $\Delta T_c$ ). The minimum rotational speed for CFC, at which the capsule was completely coated, was recorded as  $S_{min}$ , while the maximum speed of the self-made centrifugal device was 3000 rpm. The centrifugal pressure ( $P_c$ ) was calculated using Eq. (1), where  $m$  is the weight of the film,  $S$  is the rotational speed,  $r$  is the radius of the centrifugal ring, and  $A_f$  is the area of the film. The minimum centrifugal pressure ( $P_{cmin}$ ) and operating centrifugal pressure range ( $\Delta P_c$ ) were calculated accordingly.

$$P_c \text{ (kPa)} = \frac{m \times (2\pi \times S)^2 \times r}{A_f} \quad (1)$$

### 2.5. Rheological study

For the polymer films, the melt rheological behavior was determined using a rheometer (HR-1, TA Instruments, New Castle, DE, USA) with a 25.0 mm parallel plate at a testing gap of 120  $\mu\text{m}$ . The polymer films were cut into circles, loaded onto the preheated platform, and maintained at 180 °C for 120 s. The viscosity was determined in flow mode from 180 °C to 30 °C (−5 °C/min), using a constant shear rate of 5  $\text{s}^{-1}$ . The temperature-viscosity curves were recorded, and the temperature at which tangents of high and low viscosity zones intersected was recorded as the soft temperature ( $T_s$ ).

The loaded samples were maintained at 35 °C for 120 s, and then the storage modulus ( $G'$ ) and loss modulus ( $G''$ ) were determined in an oscillation mode from 35 °C to 100 °C (5 °C/min) at a frequency of 1 Hz and a strain of 1% (linear viscoelastic regime). The temperature-modulus curves were recorded, and the temperature at which  $G'$  and  $G''$  intersect was recorded as the viscous flow temperature ( $T_f$ ).

### 2.6. Mechanical property of polymer films

For assessing the mechanical property of films, the polymer films were cut into rectangles (15.0 mm × 50.0 mm). The initial film width ( $W_0$ ) was 15.0 mm, while the initial film thickness ( $T_0$ ) was determined using an electronic micrometer. The mechanical property of the films

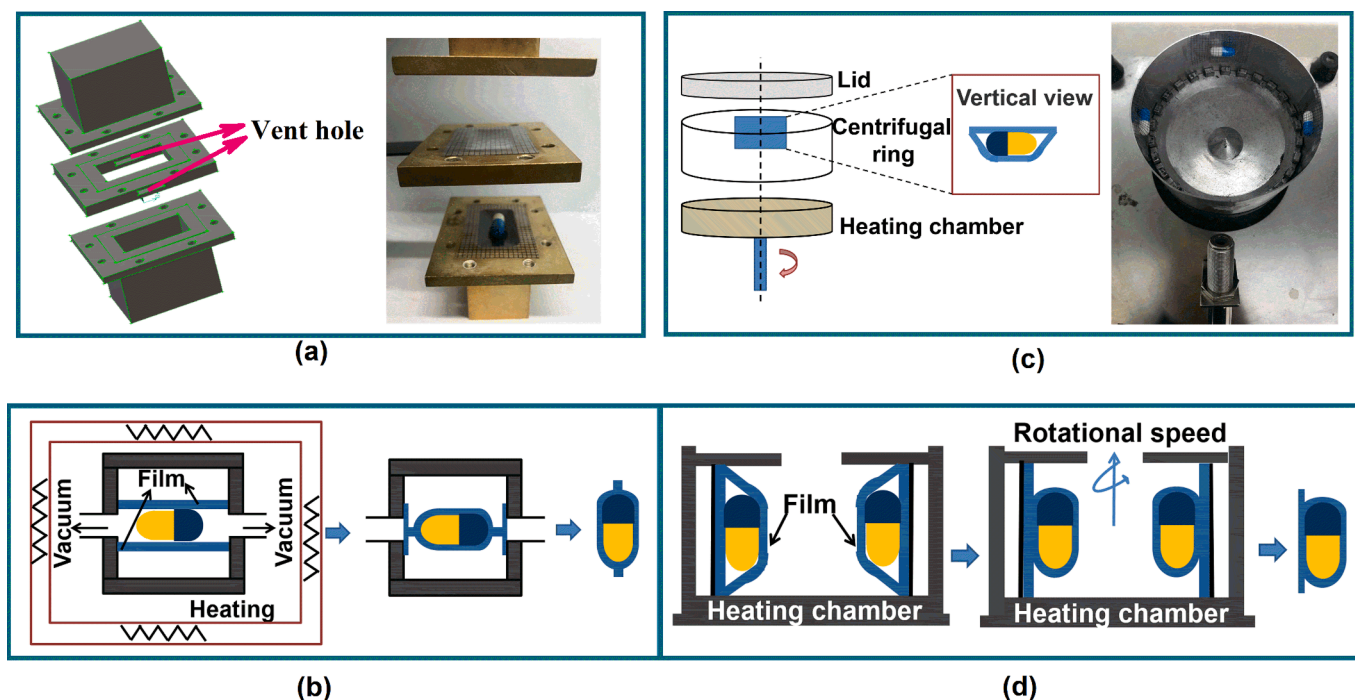


Fig. 1. (a) Design and operation of the self-made mold and (b) schematic diagram of vacuum forming coating; (c) design and operation of the self-made mold and (d) schematic diagram of centrifugal forming coating.

was measured at different temperatures (20, 45, 70, and 95 °C) using a universal testing machine (Instron5966, Instron Corporation, Norwood, MA, USA). The initial film length was 20.0 mm, and the tensile speed was 1.00 mm/s. The ultimate load ( $F_{max}$ ) was recorded to calculate the tensile stress at break ( $\sigma_b$ ) based on Eq. (2).

$$\sigma_b \text{ (MPa)} = \frac{F_{max}}{W_0 \times T_0} \quad (2)$$

## 2.7. Appearance and microstructure

Film deformation during the VFC and CFC processes was visually inspected. Red pigment (approximately 2 mg) was added to the capsule core to visualize the dissolution process of the VFC capsule. The VFC capsule was withdrawn during dissolution and blotted dry, and the pigment diffusion behavior was visually examined to evaluate the coating integrity. A vertical section of the film junction microstructure, before and after complete fusion, was assessed by scanning electron microscopy (SEM, TM-1000, Hitachi, Tokyo, Japan). Samples were sputter-coated with gold using a sputter coater (E-1010, Hitachi).

## 2.8. In vitro dissolution

The *in vitro* dissolution of VFC and CFC capsules was determined using the basket method (USP Apparatus I) at 75 rpm. The dissolution medium was 500 mL distilled water at  $37 \pm 0.5$  °C. Two capsules (containing about 100 mg MT) were placed into each basket, and 10 mL samples were withdrawn and replenished with a fresh medium at predetermined time intervals. The solution was filtered through a 0.45  $\mu$ m microporous membrane and assayed at 274 nm using a UV-vis spectrophotometer (UV-2450, Shimadzu, Tokyo, Japan). The cumulative drug release ( $Q$ ) was calculated using the equation generated from the calibration curve ( $A = 0.0041 C - 0.0008$ ,  $R = 0.9997$ ), where  $A$  was absorption and  $C$  was drug concentration ( $\mu$ g/mL).

## 3. Results and discussion

### 3.1. Optimization of thermoforming coating operating temperature

Compared with crystalline polymers, amorphous polymers (e.g., RL and RS) present a gentle drop in modulus at the glass transition temperature ( $T_g$ ) and a wider region of sufficient stiffness (Seefried et al., 2016); therefore, they are considered suitable candidate materials for thermoforming. Using RS/RL as polymer and TEC as the plasticizer, the operating temperature was optimized for the thermoforming coating. VFC capsules coated at a constant  $P_v$  of 100 kPa using polymer film with 20% TEC (Rx2) as an example are shown in Fig. 2a. On increasing the temperature from 60 °C to 68 °C, the film deformation gradually increased; this is because a higher temperature improved the flexibility of the polymer chains and facilitated thermoforming. At 60 °C, the film remained unaltered, deforming at 65 °C under  $P_v$ . In the temperature

range of 68 °C to 88 °C (result not shown), the films deformed and fused at the junction, resulting in a well-integrated coating. However, at a markedly high temperature (90 °C), the film sagged under the gravity of the capsule without baffle support (Fig. S1a vs. Fig. S1b). Therefore, the operating temperature ranged from 68 °C to 88 °C ( $\Delta T_v = 20$  °C), at which the VFC capsules presented a smooth surface and satisfactory integrity.

A low  $T_{vmin}$  was important to ensure the stability of the capsule core during VFC, and a wide  $\Delta T_v$  was preferred to maintain consistent operation. The effect of the TEC concentration (Rx1–4) on the operating temperature of the VFC process is shown in Fig. 2b. When an insufficient TEC concentration (10%) was added,  $T_{vmin}$  was 100 °C, at which the gelatin shells inside were thermally unstable. By increasing the TEC concentration from 15 to 30%, the  $T_{vmin}$  decreased from 88 °C to 52 °C, whereas  $\Delta T_v$  initially increased from 7 °C to 20 °C and then remained at approximately 18 °C. Considering that the  $T_g$  affects the thermoforming temperature (Cha et al., 2020), the influence of TEC concentration on  $T_g$  was shown in Fig. S2. On elevating the TEC concentration, TEC incorporation into the long chains of RS/RL polymers can increase the free volume between polymer chains and promote polymer chain movement (Yang et al., 2015), resulting in a reduced  $T_g$  (Fig. S2b) and lower operating temperature. On increasing the TEC concentration from 15 to 30%, the  $T_g$  decreased from 49.7 °C to 37.2 °C, whereas the  $T_{vmin}$  decreased from 88 °C to 52 °C. With increased TEC concentrations, the increased temperature required for thermoforming above  $T_g$  decreased from 38.3 °C to 14.8 °C. This was attributed to the accelerated flexibility of the polymer chain with more TEC.

CFC capsules coated at a constant rotational speed of 3000 rpm using a polymer film with 20% TEC (Rx2) as an example are shown in Fig. 3a. At low operating temperatures of 70 °C and 80 °C, the film deformation was insufficient to produce an integrated coating. At increased operation temperatures (85–115 °C), film deformation and fusion were easier, resulting in an integrated coating. However, at a markedly high temperature of 120 °C, the hard gelatin shell inside was deformed. A low  $T_{cmin}$  and a high  $\Delta T_c$  were preferred to ensure the capsule core stability and CFC coating operability. Therefore, different TEC concentrations (Rx1–4) were added to regulate the operating temperatures of the CFC process. As shown in Fig. 3b, increasing the TEC concentration from 15 to 30% reduced the  $T_{cmin}$  from 105 °C to 60 °C. After incorporating the plasticizer, the flexibility of the polymer chain accelerated, and the thermoforming temperature of CFC was reduced. Given the capsule core stability, the  $T_{cmax}$  of the CFC process was unaltered (115 °C). Therefore, the  $\Delta T_c$  increased from 10 °C to 55 °C when the TEC concentration was increased, indicating an improved CFC operability.

### 3.2. Optimization of thermoforming coating operating pressure

Using  $T_{vmin}$  as the operating temperature, the effect of the TEC concentration on the operating  $P_v$  of the VFC process is shown in Fig. 4a. Increasing the TEC concentration from 15 to 20% resulted in an obvious decrease in  $P_{vmin}$  from 82 kPa to 28 kPa. Increasing TEC to 30% slightly

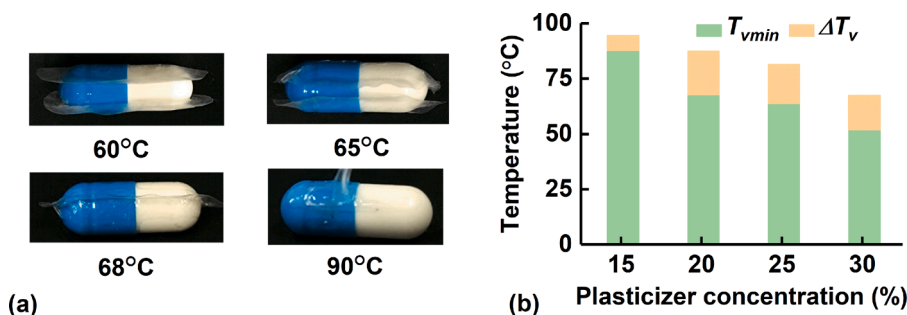


Fig. 2. (a) Deformation of the polymer film with 20% plasticizer at different temperatures and (b) the effect of plasticizer concentration on the operating temperature of the VFC process. VFC, vacuum forming coating.

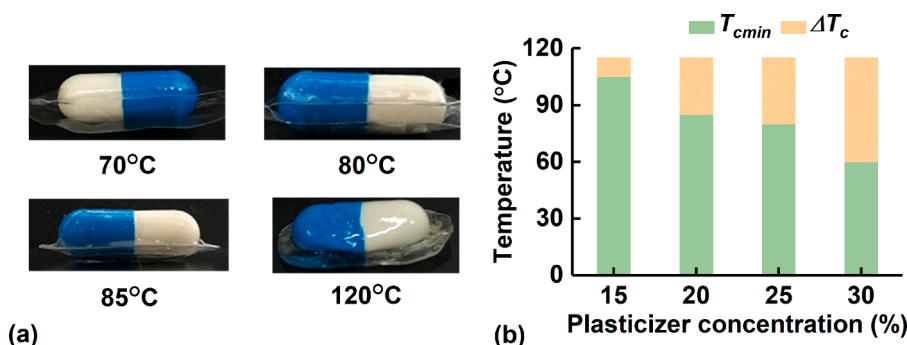


Fig. 3. (a) Deformation of polymer film (Rx2) at different temperatures and (b) the effect of plasticizer concentration on the operating temperature of the CFC process. CFC, centrifugal forming coating.

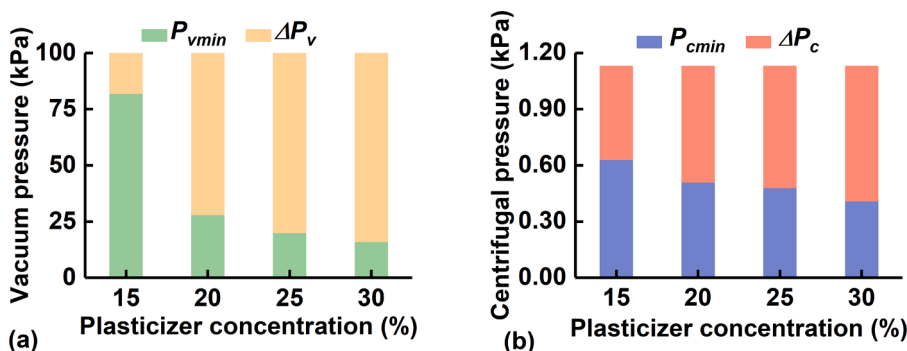


Fig. 4. Effect of plasticizer concentration on the (a) operating vacuum pressure of the VFC process and (b) operating centrifugal pressure of the CFC process. VFC, vacuum forming coating; CFC, centrifugal forming coating.

decreased the  $P_{vmin}$  to 16 kPa. These results suggested that the polymer film with 15% TEC was partially plasticized, requiring a considerably higher pressure for deformation. However, the films with more than 20% TEC were almost completely plasticized and could thermoform under low pressure. In addition, the  $\Delta T_v$  of films with 20–30% TEC (72–84 kPa) was substantially higher than that of the film with 15% TEC (18 kPa).

Using the  $T_{cmin}$  as the operation temperature, the effect of TEC concentrations on the operating centrifugal pressure during the CFC process was evaluated (Fig. 4b). Upon increasing the TEC concentration from 15 to 30%, the  $P_{cmin}$  decreased from 0.63 kPa to 0.41 kPa. The maximum centrifugal pressure was 1.13 kPa due to the limited rotational speed of the device (3000 rpm). Therefore, increasing the TEC concentration, elevated  $\Delta P_c$  from 0.50 kPa to 0.72 kPa.

Using polymer films (Rx1–4) as thermoforming materials, the two thermoforming coating processes, CFC and VFC, were compared. On the one hand, the determined  $T_{cmin}$  (105–60 °C) in Fig. 3b was much higher than the determined  $T_{vmin}$  (88–52 °C) in Fig. 2b. This is because the  $P_c$  applied to the polymer film was much lower than the applied  $P_v$ . Therefore, a higher temperature is necessary to obtain the required film ductility and formability. Furthermore, the operating temperature during CFC was determined in the heating chamber (Fig. 1c), which was higher than the actual temperature of the polymer film. In addition, the  $\Delta T_c$  of the CFC process is much wider than the  $\Delta T_v$  of the VFC process. For example, the  $\Delta T_c$  and  $\Delta T_v$  values of Rx2 were 35 °C and 20 °C, respectively. As the  $T_{cmax}$  was much higher than the  $T_{vmax}$ , the film could better withstand higher temperatures during the CFC process (with a baffle to prevent the film from sagging) than during the VFC process (no baffle to prevent the film from sagging). Conversely, the  $P_{cmin}$  in the CFC process was much lower than that in the VFC process. The  $T_{cmin}$  of CFC was higher than that of VFC, resulting in increased polymer chain flexibility and decreased pressure required for thermoforming.

### 3.3. Influence of TEC concentration on rheological and mechanical behaviors of the RS/RL films

A steady rheology test was conducted at a constant shear rate of  $5 \text{ s}^{-1}$  to evaluate the melt viscosity. The temperature-viscosity curves of the polymer films with different TEC concentrations (Rx1–4) are shown in Fig. 5a. At TEC concentrations ranging between 15 and 30%, the film viscosity was low at temperatures above the  $T_s$  but was abruptly elevated at temperatures below the  $T_s$ . The viscosity-increasing rates of films with different TEC concentrations were similar during cooling. As shown in Fig. 5b, increasing the TEC concentration from 15 to 30% could decrease the  $T_s$  from 85.9 °C to 53.6 °C, facilitating the thermoforming coating process. During the VFC process, the  $T_s$  values of the polymer films approximated their  $T_{vmin}$  values (Fig. 2b), suggesting that the  $T_s$  of the polymer films could be used to predict the  $T_{vmin}$ . When the viscosity was lower than the critical viscosity (approximately  $5 \times 10^4 \text{ Pa}\cdot\text{s}$ ) at the  $T_s$ , the polymer material would possess sufficient fluidity for thermoforming coating. The critical viscosity was within the thermoformable viscosity range reported in the literature (Münstedt et al., 2006), where polyethylene and polypropylene were used as polymer materials.

A dynamic rheology test was performed at a frequency of 1 Hz to evaluate the modulus. The temperature-modulus curves of polymer films with different TEC concentrations (Rx1–4) are shown in Fig. 6. For the polymer film, both  $G'$  and  $G''$  decreased with increasing temperature. For the film with 15% TEC, the  $T_f$  was 85.2 °C, at which both  $G'$  and  $G''$  were 12.8 kPa. On further increasing the TEC concentration from 20 to 30%, the  $T_f$  decreased from 72.3 °C to 57.3 °C, whereas the corresponding modulus increased from 18.3 kPa to 28.9 kPa. Considering that  $T_f$  is the critical temperature at which the material changes from the rubbery state ( $G' > G''$ ) to a viscous state ( $G' < G''$ ), a low  $T_f$  indicates a low operating temperature for the thermoforming coating process. At a constant temperature of 50 °C, increasing the TEC concentration from 15 to 20% could decrease the  $G'$  and  $G''$  from 81.2 kPa to 44.5 kPa and

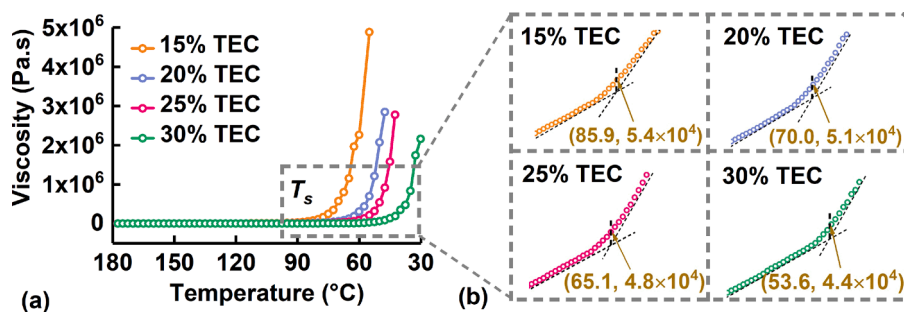


Fig. 5. The effect of TEC concentration on (a) temperature-viscosity curves and (b) T<sub>s</sub> of polymer films. TEC, triethyl citrate; T<sub>s</sub>, soft temperature.

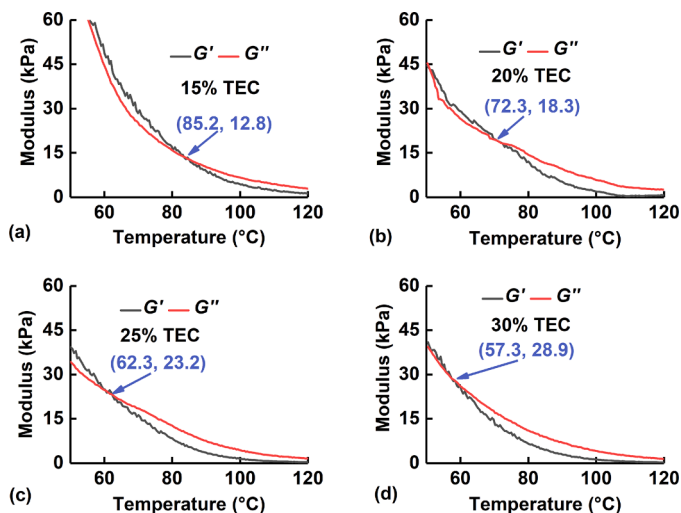


Fig. 6. The effect of TEC concentration on temperature-modulus curves: (a) 15%, (b) 20%, (c) 25%, and (d) 30%. TEC, triethyl citrate.

from 84.1 kPa to 45.3 kPa, respectively. Upon further increasing the TEC concentration to 25 and 30%, G' and G'' were almost identical (approximately 40 kPa). This suggests that an additional 20% TEC concentration was sufficient for polymer plasticization. The operating temperature of the thermoforming coatings should be near or higher than the T<sub>f</sub>. Therefore, the T<sub>min</sub> (88, 68, 64, and 52 °C, Fig. 2b) of the film with 15–30% TEC was near their T<sub>f</sub>, whereas the T<sub>min</sub> (105, 85, 80, and 60 °C, Fig. 3b) of the film with 15–30% TEC was considerably higher. Furthermore, the modulus at T<sub>f</sub> (G' = G'') increased from 12.8 kPa to 28.9 kPa upon increasing the TEC concentration. Upon increasing the TEC concentrations, the T<sub>f</sub> decreased while the corresponding modulus increased, suggesting that temperature had a greater influence on the film modulus than the TEC concentration.

A tensile test was conducted to investigate the effect of TEC concentrations and temperatures on the mechanical property of the polymer films (RS:RL = 8:2) with a constant film thickness of approximately 0.15 mm. As shown in Fig. 7a, increasing the TEC concentration from 15 to 20% decreased the σ<sub>b</sub> from 3.70 MPa to 2.45 MPa. Further increasing the TEC concentration to 25 and 30% only marginally decreased the σ<sub>b</sub> to 2.20 MPa and 2.11 MPa, respectively. These findings revealed that 20% TEC was sufficient for complete polymer plasticization, minimizing the mechanical strength of the film and facilitating the thermoforming coating process. Furthermore, these results are consistent with the results shown in Fig. 4a and b. The film with 20% TEC was further used in Fig. 7b, at a temperature (20 °C) below the T<sub>g</sub> (45.7 °C), σ<sub>b</sub> of the polymer film (Rx2) was high (2.5 MPa). This can be attributed to the restricted motion of the chain segment, enabling the fixation of the temporary shape (Wu et al., 2020). At temperatures (45 °C and 70 °C) near and above the T<sub>g</sub> (45.7 °C), the σ<sub>b</sub> decreased to 0.2 MPa and 0.1

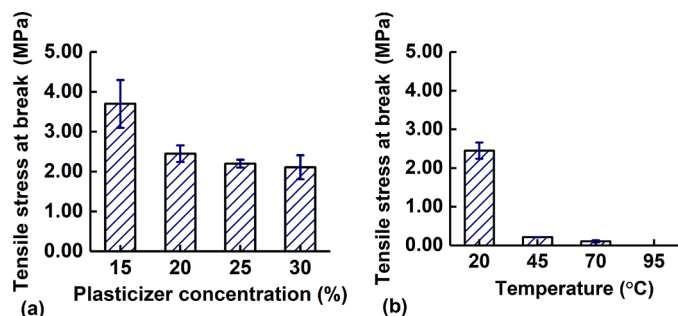


Fig. 7. Effect of (a) TEC concentrations and (b) temperatures on the mechanical property of the polymer film (n = 3). TEC, triethyl citrate.

MPa, which can be attributed to the good mobility of the polymer chain segments, enabling conformational changes. At a temperature (90 °C) above the T<sub>f</sub> (72.3 °C), no σ<sub>b</sub> was determined, as the polymer film was in the viscous state, and the F<sub>max</sub> during the tensile test was extremely low to be determined. At higher temperatures, the mechanical strength of the polymer film decreased, and the minimum pressure required for film deformation was reduced. This could explain the results in Fig. 4a and b, where the P<sub>min</sub> was much higher than the P<sub>min</sub> because the T<sub>min</sub> was lower than the T<sub>min</sub>.

#### 3.4. Influence of RS/RL ratio and film thickness on *in vitro* dissolution

The effect of the RS/RL ratio (Rx5, Rx2, and Rx6) on the *in vitro* dissolution of the VFC capsules was evaluated at a constant film thickness of approximately 0.15 mm and 20% TEC (Fig. 8a). At the RS/RL ratios of 9:1 and 8:2, the sustained-release behavior lasted for 24 h, presenting Q<sub>24h</sub> of 84.8% and 91.6%, respectively. At an RS/RL ratio of 5:5, the drug release was rapid (Q<sub>4h</sub> = 54.7%), and the sustained-release behavior lasted for 12 h (Q<sub>12h</sub> = 95.2%). The drug release from VFC capsules accelerated with increased RL in the coating, as the RL polymer possesses a higher number of quaternary ammonium groups, which increased the swelling capacity and water permeability (Pearnchob and Bodmeier, 2003). Similarly, the effect of the RS/RL ratio on the *in vitro*

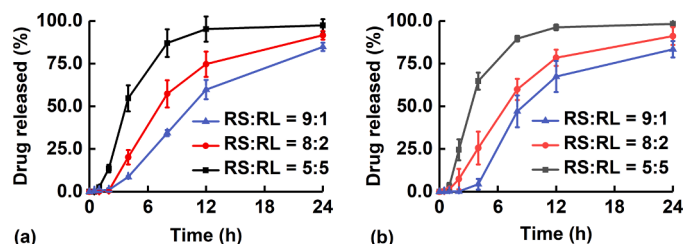


Fig. 8. Influence of the RS/RL ratio on the dissolution of the (a) VFC and (b) CFC capsules (n = 6). VFC, vacuum forming coating; CFC, centrifugal forming coating.

dissolution of CFC capsules with a film thickness of approximately 0.15 mm and 20%TEC is shown in Fig. 8b. The higher the RL concentration in the coating, the faster the drug release from CFC capsules. Therefore, the optimal RS/RL ratio for both VFC and CFC capsules was 8:2, at which the sustained-release behavior lasted for 24 h, with a high cumulative drug release.

The effect of film thickness (Rx7, Rx2, and Rx8) on the *in vitro* dissolution of the VFC capsules is shown in Fig. 9a. The film thickness of polymer films prepared by different formulations was shown in Table S1. At a film thickness of 0.10 mm, the drug release was rapid ( $Q_{4h} = 65.8\%$ ), and the sustained-release behavior lasted for 12 h ( $Q_{12h} = 93.6\%$ ). When the film thickness was 0.15 mm, the sustained-release behavior lasted for 24 h ( $Q_{24h} = 91.6\%$ ). On further increasing the thickness to 0.20 mm, the dissolution behavior was slowed, and the cumulative drug release was incomplete at 24 h ( $Q_{24h} = 78.3\%$ ). The results were similar to those reported in the literature (Ammar et al., 2016), where increasing the coating thickness resulted in a marked delay in drug release. The relationship between the film thickness and average drug release rate ( $dQ/dt$ ) of the VFC capsules within 8 h was evaluated (Fig. 9c). On increasing the film thickness from 0.10 mm to 0.20 mm, the  $dQ/dt$  of the VFC capsules decreased from 11.3%/h to 2.6%/h. The results can be explained by Fick's diffusion equation (Yang et al., 2018) (Eq. (3)), where  $A_s$  is the surface area,  $D$  is the diffusion coefficient,  $K$  is the drug distribution coefficient between the film and core,  $\Delta C$  is the drug concentration difference inside and outside the coating, and  $d$  is the coating thickness. For the VFC capsules,  $A_s$ ,  $D$ ,  $K$ , and  $\Delta C$  remained constant during the 8 h of testing; therefore,  $dQ/dt$  negatively correlated with  $d$ , which was affected by the film thickness.

$$\frac{dQ}{dt} = \frac{A_s \times D \times K \times \Delta C}{d} \quad (3)$$

Similarly, the influence of film thickness on the *in vitro* dissolution of CFC capsules is shown in Fig. 9b. Drug release slowed down with an increase in film thickness from 0.10 mm to 0.20 mm. Like VFC capsules, the optimal film thickness of CFC capsules was 0.15 mm, at which a sustained-release behavior over 24 h was obtained. The relationship between film thickness and the average  $dQ/dt$  of the CFC capsules during 8 h is shown in Fig. 9c. Upon increasing the film thickness from 0.10 mm to 0.20 mm, the  $dQ/dt$  of the CFC capsules decreased from 9.1%/h to 1.6%/h.

### 3.5. Deformation of polymer film and thickness distribution of coating

RS/RL films (Rx2), with 2 mm × 2 mm grids, were used to visually evaluate polymer film deformation during the VFC and CFC processes (Fig. 10a). For VFC capsules, the grids at the top were unaltered, but the grids at the junction in the *x*- and *y*-axis directions were 1.2 and 1.5 times longer, respectively. This indicated that biaxial stretching was the dominant deformation observed in the polymer film during the VFC process (Ghobadnam et al., 2014). For the CFC capsules, the grids at the top and the junction in the *x*-axis direction were unaltered. However, the

grids at the junction in the *y*-axis direction were 2.0 times longer only at the side close to the heating chamber. The uniaxial stretching in the *y*-axis direction is related to the non-uniform temperature field during the CFC process.

At the points of "A", "A'", "a" and "a'", the thickness of two isolated films coupled was measured. For the VFC capsules, the coating thickness at points "A", "A'", "a", and "a'" was half of the determined thickness. For the CFC capsules, the coating thickness at points "A", "A'", "a", and "a'" were calculated by subtracting the thickness of film near the baffle from the measured thickness of coupled. At the other points ("B", "B'", "b", "b'" and so on), the thickness of the capsule shell was subtracted in thickness calculation. The coating thickness distribution along the *x*-axis is shown in Fig. 10b. For VFC capsules, the coating thickness at the top (positions D and d) was approximately 0.15 mm. The coating thickness at the capsule body (position d) was marginally less than that at the capsule cap (position D). This can be attributed to the greater distance between the polymer film and the capsule body, which resulted in increased film deformation. Moreover, the coating thickness at the capsule cap decreased from 0.14 mm to 0.12 mm (from position C to A), while the coating thickness at the capsule body decreased from 0.13 mm to 0.11 mm (from position c to a). This indicated that the polymer film stretched more at the joint area than at the top. For CFC capsules, the polymer film at the top area (positions D and d) demonstrated almost no stretching at a coating thickness of approximately 0.15 mm. In contrast, the coating thickness at both, the capsule cap (from position C to B) and body (from position c to b) decreased from 0.13 mm to 0.12 mm. However, the polymer film at the junction area (positions A and a) showed no stretching (coating thickness ≈ 0.15 mm) as the two films were fixed together at the junction area before the CFC process.

The coating thickness distribution in the middle of the VFC and CFC capsules (in the capsule body) along the *y*-axis direction is shown in Fig. 10c. For VFC capsules, the polymer film at the top area (position D') did not stretch (coating thickness ≈ 0.15 mm). In contrast, the coating thickness gradually and symmetrically decreased from 0.13 mm to 0.11 mm from the top area (position D') to the junction area at both sides (positions A' and a'). The symmetrical stretching was attributed to the uniform temperature field during the VFC process, classified as a symmetrical thermoforming coating technique. For CFC capsules, the polymer film from the top area (position D') to the junction area, on the side far away from the heating chamber (position a'), revealed no stretching (coating thickness ≈ 0.15 mm). However, the coating thickness decreased from 0.15 mm to 0.07 mm from the top area (position D') to the junction area at the side close to the heating chamber (position A'). The asymmetrical stretching was attributed to the non-uniform temperature field during the CFC process, classified as an asymmetrical thermoforming coating technique.

### 3.6. Coating integrity and dissolution mechanism

We compared the coating integrity after thermoforming using VFC capsules coated with the optimal film (Rx2) as a specimen (Fig. 11a–b).

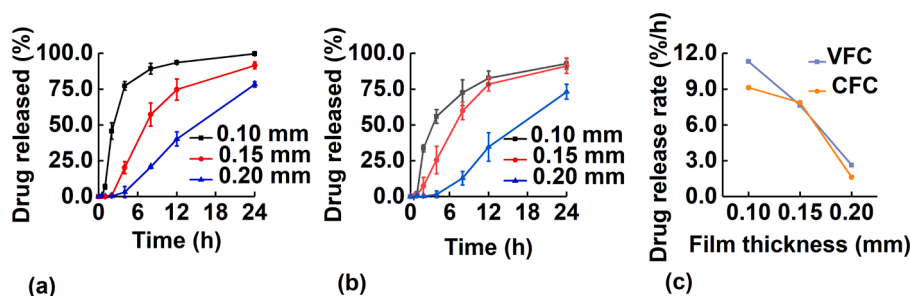


Fig. 9. The effect of film thickness on the dissolution of the (a) VFC and (b) CFC capsules; (c) the relationship between the film thickness and the drug release rate of the VFC and CFC capsules ( $n = 6$ ). VFC, vacuum forming coating; CFC, centrifugal forming coating.

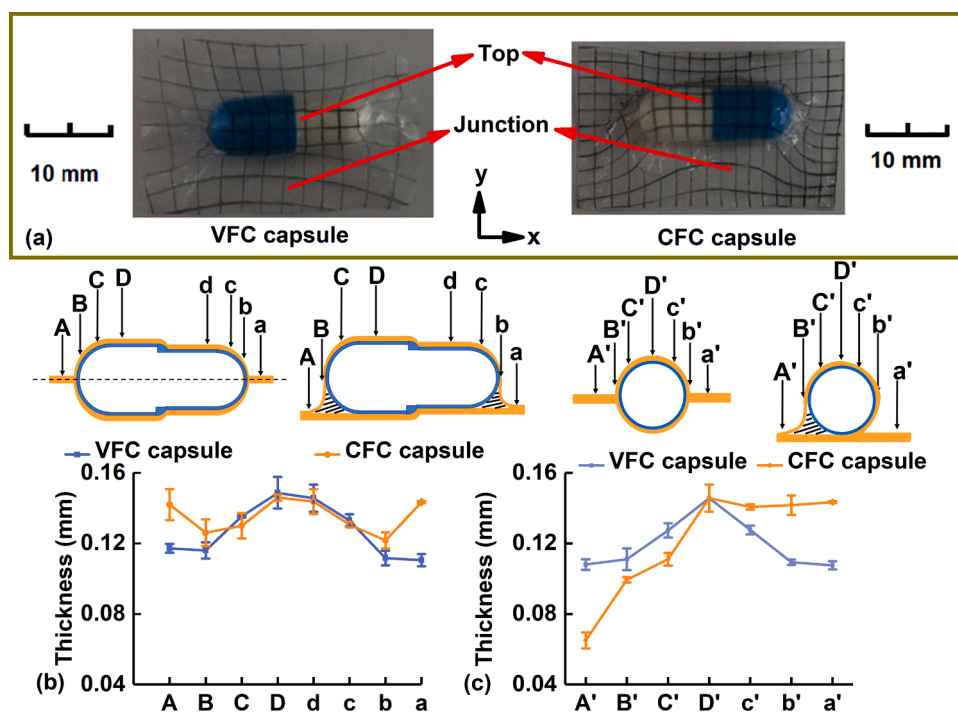


Fig. 10. (a) Deformation of polymer film and thickness distribution of the coating in the (b) x-axis and (c) y-axis directions ( $n = 3$ ).

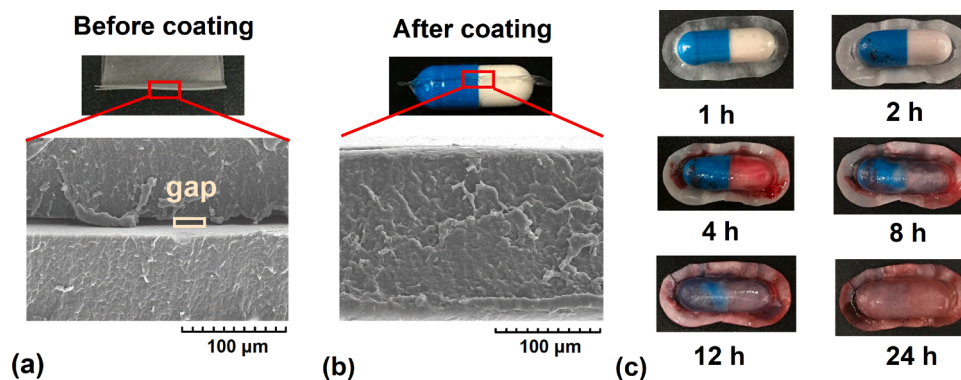


Fig. 11. Microstructure of the junction area of the VFC capsule (a) before and (b) after coating; (c) appearance of the VFC capsule during dissolution. VFC, vacuum forming coating.

An obvious gap in the junction area between the two films was observed before the VFC process. After the VFC process, the junction area of the two films entirely fused, suggesting that the coating of the VFC capsules was complete. To further evaluate the coating integrity, a red pigment was added to the optimal VFC capsule to visualize the *in vitro* dissolution process (Fig. 11c). No pigment was released within 1 h, during which the coating was swollen, and water was found to penetrate the coating. During the 2–12 h period, the pigment gradually released through the coating, with no release channel detected at the junction area of the VFC capsules. The inside pigment and hard gelatin shell were completely released from the coated capsule within 24 h, leaving an integrated coating shell.

As shown in Fig. 12, there was a visible sealing ring around the optimal VFC and CFC capsules to maintain a sufficient junction area for the integrated coating. The ring with a width of 0.5–1.0 mm was flexible, with no potential for damaging mucous membranes (Yuan et al., 2019). Both VFC and CFC capsules coated with the optimal film (Rx2) exhibited a 24 h sustained-release behavior. However, the lag time of the VFC capsules was approximately 2 h ( $Q_{2h} = 0.7\%$ ), while the lag time of the CFC capsules was approximately 1 h ( $Q_{1h} = 1.4\%$ ). This is because

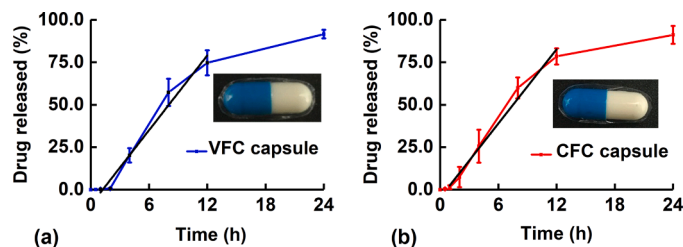


Fig. 12. The appearance and dissolution behavior of the optimal (a) VFC and (b) CFC capsules ( $n = 6$ ). VFC, vacuum forming coating; CFC, centrifugal forming coating.

pore formation induced by polymer swelling and water permeation requires time. The dissolution behavior of the VFC and CFC capsules can be further explained using biphasic drug release behaviors based on Fick's diffusion law (Yang et al., 2018). According to Eq. (3) in Section 3.5, the  $\Delta C$  of 1–12 h was constant because the solution inside the coating was saturated, and the concentration of the drug outside the

coating was relatively low. Therefore, the release dissolution was fitted using a zero-order equation and the results were as follows:  $y = 7.34x - 9.00$  ( $R = 0.985$ ) for VFC capsules;  $y = 7.29x - 4.79$  ( $R = 0.990$ ) for CFC capsules. The average  $dQ/dt$  values of the VFC and CFC capsules were 7.34%/h and 7.29%/h, respectively. The  $dQ/dt$  was obviously decreased after 12 h, and it was attributed to the decrease of drug concentration difference inside and outside the coating ( $\Delta C$ ) with more drugs released out of the capsule.

#### 4. Conclusion

In the present study, capsules were successfully coated using the VFC and CFC techniques, demonstrating a 24 h sustained-release behavior. This indicates that the thermoforming coating techniques are solvent-free methods to prepare functional capsule coatings. At higher temperatures and TEC concentrations, the viscosity and modulus of the RS/RL films were decreased, which enhanced the coating integrity. Therefore, increasing the TEC concentration could effectively decrease the minimum operating temperature and pressure. According to the linear correlation between the drug release rate and film thickness, the drug dissolution behavior could be regulated and predicted by altering the film thickness. With a uniform temperature field, the VFC technique presented a better coating uniformity and was classified as the symmetrical thermoforming coating technique. Thermoforming coating techniques could be used in a galenic pharmacy environment or for small clinical batches preparation, although the stability of the coating and the scale-up of processes should be further studied. In addition, the easiness of the process suggested these thermoforming coating techniques have advantages in the small-scale personalized coating of oral solid preparations. Additional coating materials (i.e., ethylcellulose, Eudragit® EPO, and Eudragit® L100-55) and solid preparations (i.e., tablets and pellets) should be further investigated to improve the application of thermoforming coating techniques in the field of biomedicine.

#### CRediT authorship contribution statement

**Lian Shen:** Methodology, Formal analysis, Investigation, Data curation, Writing – original draft, Writing – review & editing. **Xiaohong Yu:** Formal analysis, Data curation, Writing – review & editing. **Hui Fu:** Data curation, Writing – review & editing, Funding acquisition. **Sainan Wei:** Conceptualization, Methodology, Writing – review & editing. **Weiguang Shan:** Conceptualization, Writing – review & editing, Funding acquisition. **Yan Yang:** Conceptualization, Methodology, Formal analysis, Investigation, Data curation, Writing – original draft, Writing – review & editing, Funding acquisition.

#### Declaration of Competing Interest

The authors declared that they have no conflicts of interest to this work.

#### Acknowledgments

This work has been supported by the Zhejiang University of Technology Project [KYY-HX-20210634, YX-[2015]001@] and the Foundation of Zhejiang Educational Committee [Y201738311].

#### Supplementary materials

Supplementary material associated with this article can be found, in the online version, at doi:10.1016/j.ejps.2021.106050.

#### References

- Ammar, H.O., Ghorab, M.M., Felton, L.A., Gad, S., Fouly, A.A., 2016. Effect of antiadherents on the physical and drug release properties of acrylic polymeric films. *AAPS PharmSciTech* 17 (3), 682–692. <https://doi.org/10.1208/s12249-015-0397-7>.
- Bose, S., Bogner, R.H., 2007. Solventless pharmaceutical coating processes: a review. *Pharm. Dev. Technol.* 12 (2), 115–131. <https://doi.org/10.1080/10837450701212479>.
- Bose, S., Bogner, R.H., 2010. Solventless visible light-curable coating: I. Critical formulation and processing parameters. *Int. J. Pharm.* 393 (1–2), 32–40. <https://doi.org/10.1016/j.ijpharm.2010.01.041>.
- Cha, J., Kim, M., Park, D., Go, J.S., 2019. Experimental determination of the viscoelastic parameters of K-BKZ model and the influence of temperature field on the thickness distribution of ABS thermoforming. *Int. J. Adv. Manuf. Tech.* 103 (1–4), 985–995. <https://doi.org/10.1007/s00170-019-03408-8>.
- Cha, J., Song, H.Y., Hyun, K., Go, J.S., 2020. Rheological measurement of the nonlinear viscoelasticity of the ABS polymer and numerical simulation of thermoforming process. *Int. J. Adv. Manuf. Tech.* 107 (5–6), 2449–2464. <https://doi.org/10.1007/s00170-020-04979-7>.
- Deshmukh, R., Harwansh, R.K., Das Paul, S., Shukla, R., 2020. Controlled release of sulfasalazine loaded amidated pectin microparticles through Eudragit S 100 coated capsule for management of inflammatory bowel disease. *J. Drug Deliv. Sci. Technol.* 55, 101495. <https://doi.org/10.1016/j.jddst.2019.101495>.
- Erdogan, E.S., Eksi, O., 2014. Prediction of wall thickness distribution in simple thermoforming moulds. *Stroj. Vestn. J. Mech. Eng.* 60 (3), 195–202. <https://doi.org/10.5545/sv-jme.2013.1486>.
- Ghobadnam, M., Mosaddegh, P., Rezaei Rejani, M., Amirabadi, H., Ghaei, A., 2014. Numerical and experimental analysis of HIPS sheets in thermoforming process. *Int. J. Adv. Manuf. Tech.* 76 (5–8), 1079–1089. <https://doi.org/10.1007/s00170-014-6329-y>.
- Hoffmann, E.M., Breitenbach, A., Breikreutz, J., 2011. Advances in orodispersible films for drug delivery. *Expert Opin. Drug Deliv.* 8 (3), 299–316. <https://doi.org/10.1517/17425247.2011.553217>.
- Hosseini, H., Berdyshev, B.V., Mehrabani-Zeinabad, A., 2007. Modeling of deformation processes in vacuum thermoforming of a pre-stretched sheet. *Polym. Plast. Technol. Eng.* 45 (12), 1357–1362. <https://doi.org/10.1080/03602550600948731>.
- Hosseini, H., Berdyshev, B.V., Mehrabani-Zeinabad, A., 2010. Rheological modeling of extrusion in plug-assisted vacuum thermoforming. *J. Appl. Polym. Sci.* 117 (1), 171–177. <https://doi.org/10.1002/app.31963>.
- Lee, J.K., Scott, C.E., Virkler, T.L., 2001a. Effects of rheological properties and processing parameters on ABS thermoforming. *Polym. Eng. Sci.* 41 (2), 240–261. <https://doi.org/10.1002/pen.10725>.
- Lee, J.K., Virkler, T.L., Scott, C.E., 2001b. Influence of initial sheet temperature on ABS thermoforming. *Polym. Eng. Sci.* 41 (10), 1830–1844. <https://doi.org/10.1002/pen.10880>.
- Leite, W.O., Rubio, J.C.C., Mata, F., Hanafi, I., Carrasco, A., 2018. Dimensional and geometrical errors in vacuum thermoforming products: an approach to modeling and optimization by multiple response optimization. *Meas. Sci. Rev.* 18 (3), 113–122. <https://doi.org/10.1515/msr-2018-0017>.
- Macchi, E., Zema, L., Pandey, P., Gazzaniga, A., Felton, L.A., 2016. Influence of temperature and relative humidity conditions on the pan coating of hydroxypropyl cellulose molded capsules. *Eur. J. Pharm. Biopharm.* 100, 47–57. <https://doi.org/10.1016/j.ejpb.2015.11.021>.
- Mohamad, A., Dashevsky, A., 2006. pH-independent pulsatile drug delivery system based on hard gelatin capsules and coated with aqueous dispersion Aquacoat® ECD. *Eur. J. Pharm. Biopharm.* 64 (2), 173–179. <https://doi.org/10.1016/j.ejpb.2006.04.006>.
- Morales, R.A., Candal, M.V., Santana, O.O., Gordillo, A., Salazar, R., 2014. Effect of the thermoforming process variables on the sheet friction coefficient. *Mater. Des.* 53, 1097–1103. <https://doi.org/10.1016/j.matdes.2013.08.009>.
- Münstedt, H., Kurzbeck, S., Stange, J., 2006. Importance of elongational properties of polymer melts for film blowing and thermoforming. *Polym. Eng. Sci.* 46 (9), 1190–1195. <https://doi.org/10.1002/pen.20588>.
- Nam, G.J., Lee, J.W., 2016. Numerical and experimental studies of 3-dimensional thermoforming process. *J. Reinf. Plast. Compos.* 20 (14–15), 1182–1190. <https://doi.org/10.1106/y2xy-q59f-bruw-jnby>.
- Pearnchob, N., Bodmeier, R., 2003. Dry powder coating of pellets with micronized Eudragit® RS for extended drug release. *Pharm. Res.* 20 (12), 1970–1976. <https://doi.org/10.1023/B:PHAM.000008044.78968.81>.
- Seefried, A., Heinle, M., Drummer, D., 2016. Mechanical properties of radiation cross linked polyamide 12 after vacuum thermoforming. *Prod. Eng. Res. Dev.* 10 (2), 119–128. <https://doi.org/10.1007/s11740-016-0663-x>.
- Tang, Y., Teng, H., Shi, Y., He, H., Zhang, Y., Yin, T., Cai, C., Tang, X., 2018. Tablets of paliperidone using compression-coated technology for controlled ascending release. *Asian. J. Pharm. Sci.* 13 (2), 143–154. <https://doi.org/10.1016/j.ajps.2017.09.005>.
- Terebesi, I., Bodmeier, R., 2010. Optimised process and formulation conditions for extended release dry polymer powder-coated pellets. *Eur. J. Pharm. Biopharm.* 75 (1), 63–70. <https://doi.org/10.1016/j.ejpb.2010.01.006>.
- Wu, W., Narayana Kurup, S., Ellingford, C., Li, J., Wan, C., 2020. Coupling dynamic covalent bonds and ionic crosslinking network to promote shape memory properties of ethylene-vinyl acetate copolymers. *Polymers* 12 (4). <https://doi.org/10.3390/polym12040983> (Basel).
- Yang, Q., Ma, Y., Zhu, J., 2015. Applying a novel electrostatic dry powder coating technology to pellets. *Eur. J. Pharm. Biopharm.* 97, 118–124. <https://doi.org/10.1016/j.ejpb.2015.10.006>.
- Yang, Y., Shen, L., Li, J., Shan, W.G., 2017. Preparation and evaluation of metoprolol tartrate sustained-release pellets using hot melt extrusion combined with hot melt

coating. *Drug Dev. Ind. Pharm.* 43 (6), 939–946. <https://doi.org/10.1080/03639045.2017.1287715>.  
Yang, Y., Shen, L., Yuan, F., Fu, H., Shan, W., 2018. Preparation of sustained release capsules by electrostatic dry powder coating, using traditional dip coating as

reference. *Int. J. Pharm.* 543 (1–2), 345–351. <https://doi.org/10.1016/j.ijpharm.2018.03.047>.  
Yuan, C., Hou, H., Qian, M., Zhang, H., Luo, C., Wang, Z., 2019. A new thermoplastic coating for osmotic pump tablets I. Development of preparation process. *Chin. J. Pharm.* 50 (1), 48–58.